Lasers in Manufacturing Conference 2021

Influence analysis of the layer orientation on mechanical and metallurgic characteristics of DED manufactured parts

Florian M. Dambietz[a,b,*], Tobias S. Hartwich[a], Julian Scholl-Corrêa[b], Peter Hoffmann[b], Dieter Krause[a]

[a]*Hamburg University of Technology, Institute of Product Development and Mechanical Engineering Design, 21073 Hamburg, Germany*
[b]*ERLAS Erlanger Lasertechnik GmbH, 91056 Erlangen, Germany*

Abstract

With an increasing trend in product individualization, manufacturing custom-designed solutions and focusing on the explicit industry's needs are crucial to the manufacturer's success. Especially within high-tech industries such as aerospace industry, high-strength, large-sized but still lightweight metal parts are required. Although the Direct-Energy-Deposition (DED)-technology offers a proven outset point for targeting this issue, there are few material-, metallurgic-, process-, and geometry specific data available to support the initial design process of such parts. This contribution presents a profound study of different steel- and aluminium materials with respect to their metallurgic and mechanical characteristics. Using a state-of-the art DED-Laser system, tensile test specimens have been manufactured with alternative layer orientations. These specimens are analyzed with regard to the required milling oversize, heat-induced stress deformation, metallurgic characteristics and their tensile characteristics. As a result of this investigation, a suitable baseline for the future generation of a DED design-by-feature catalogue is given.

Keywords: DED; Additive manufacturing; metallurgy; tensile characteristics; layer orientation

1. Introduction and Motivation

With the actual trend of globalization, modern companies are faced with an increasing challenge in market competitiveness due to an increase in product specialization and individualization as stated by VdM, 2014. In order to keep and enhance market competitiveness, being able to offer highly-individualized products for high-consuming industries such as the automotive or aerospace industry is considered as a crucial, see also Liu et al., 2017. Especially for product parts in a high force load environment, there is no way of escaping metallic parts. With technologies such as Selective-Laser-Melting (SLM), small to medium sized individualized parts can be produced from various metallic materials. This SLM technology comes with several advantages, such as high-part quality due to a high layer resolution and the possibility of processing materials which are prone to reacting with oxygen, such as titanium. As the relevant machine systems are placed within an inert

* Corresponding author.
E-mail address: florian.dambietz@tuhh.de .

atmosphere, the total lack of oxygen leads to a formation of non-oxygenized parts and therefore parts with the highest possible quality, compare Kovacs, 2018. Nevertheless, due to this placement in an inert gas box, such machine systems are strongly limited in the part size they are able to produce. Especially for parts being implanted in large size machinery, the SLM process is not feasible. Furthermore, due to the high generation resolution SLM processes aim for, the material adding rate is limited. For large sized parts, this process is economically not relevant, see also Bikas et al., 2019.

As one possible solution to this presented issue, the Direct-Energy-Deposition (DED) process is of significant interest. As this technology mainly consists of a powder nozzle followed by a coaxial laser beam, the processing area of such DED systems is only limited by the guiding machine's travel range. In the case of such a machine system being based on an articulated robotic system, the working area can reach several square meters in size. Furthermore, the material adding rates in DED processes are significantly higher than with SLM processes.

All in all, the DED process can allow for the generation of large-sized steel- or aluminium parts in a considerably small process cycle time and a high degree of individualization, compare Zhang et al, 2018.

In order to generate such individualized parts, a close knowledge of the DED process and the base materials characteristics are required. As there are very few information in the pertinent literature about the metallurgic characteristics of DED manufactured parts, this contribution is intending to address this gap by providing the gathered information based on thorough testing of DED parts. Especially the anisotropic behaviour of the parts due to alternating layer orientations within the DED process has a significant impact on the parts' tensile strength and metallurgic behaviour. Within this contribution, we intend to fill that gap of missing information with close respect to the influence of the part layer orientation for DED manufactured parts.

2. State of the Art

In the rapidly developing field of additive manufacturing, there are currently two generally different manufacturing processes, compare Farayibi et al, 2019, Selective Laser Melting (SLM) on the one hand and Direct Energy Deposition (DED) on the other. In SLM, a 3D geometry is separated into two-dimensional layers, which are then melted in a powder bed using a laser beam scanner. Due to its high accuracy, this process is particularly suitable for small parts with low wall thickness, but on the other hand is limited by the maximum installation space, which is currently 800x400x500 mm^3, stated by Weaver et al., 2019. Likewise, long processing times (for parts filling the aforementioned processing space, this processing time is in the range of days) are to be expected due to the low layer thickness. The DED, on the other hand, does not rely on a powder bed, as the metal powder is delivered to the processing location via a powder nozzle coaxial to the laser beam. Thus, the processing volume is limited only by the motion system; standard systems here range from 3000x2000x1800 mm^3 (6-axis industrial robot) for repair welding. As described in section 1, the focus for the within this contribution provided process data is based on the DED process. DED is a manufacturing process in which materials are fused layer by layer to form an object on the basis of a 3D model. It therefore belongs to the additive manufacturing processes. The term generally covers the processing of plastic, ceramics or metal. However, it is predominantly used for the latter category of materials and is therefore often equated with Direct Metal Deposition (DMD), compare Imran et al., 2011. The main component of the process is the processing head. The materials are discharged in powder or wire form through a nozzle or wire conveyor. This distinguishes the process from methods such as SLM and laser beam melting (LBM), in which the material is already present at the joining point. The majority of DED and DMD processes, respectively, use powder-based materials, see Dass and Moridi, 2019, which is why only this form will be discussed in the remainder of this paper. The typical focused energy sources are a laser, an electron beam, an electric arc or a plasma arc. When the powder hits the melt pool, which usually has a diameter of 0.25-1 mm and a depth of 0.1-0.5 mm, it is melted and solidifies as the beam moves on. The diameter and depth depend on the optical configuration of

the machine and can therefore be significantly larger. The first layer of deposited metal, also referred to as filler material, is welded onto the workpiece, also referred to as base material, and each subsequent layer then solidifies onto the filler metal, see also Gibson et al., 2015 and Imran et al., 2011. In general, parts with almost complete density (99.9% according to Caroll et al. 2015) and very good mechanical properties can be produced. Nevertheless, the material properties of DED manufactured components are highly dominated by anisotropic material properties. However, the exact causes of this anisotropy are disputed in literature. Pores as well as the material structure have a significant influence on the mechanical properties and can be the reason for the anisotropy, compare Gibson et al. 2010, Carroll et al. 2015, Wang et al. 2016, Wolff et al. 2016, Wolff et al. 2017, Saboori et al. 2020. An anisotropic or directional material microstructure occurs due to the complex temperature history introduced into a workpiece by the DED process. This in turn is influenced by many factors, such as the solidification rate, the direction of the temperature gradient and the heat dissipation. Pores that are anisotropically distributed arise primarily from bonding defects between the individual material layers. Since the formation of the pores and the temperature history are thus linked to the manufacturing directions, the mechanical properties are also dependent on the manufacturing directions. The material properties resulting from the DED process typically exhibit high tensile strength and low ductile behaviour. The highest tensile strength is usually obtained in the scan direction and the highest ductility in the build-up direction compare Gibson et al. 2010, Carroll et al. 2015, Wang et al. 2016, Wolff et al. 2016, Wolff et al. 2017, Saboori et al. 2020.

3. Layer orientation and metallurgic characteristics analysis of DED parts

For the analysis of the layer orientation of DED manufactured parts, we identified in total six different orientations. Since the material properties depend on the printing and build-up direction due to the layer-by-layer structure, as shown for example by Wolff et al., 2017, Caroll et al., 2015 and Wang et al. 2016, the in the following Figure 1 displayed orientations are considered as relevant for the analysis.

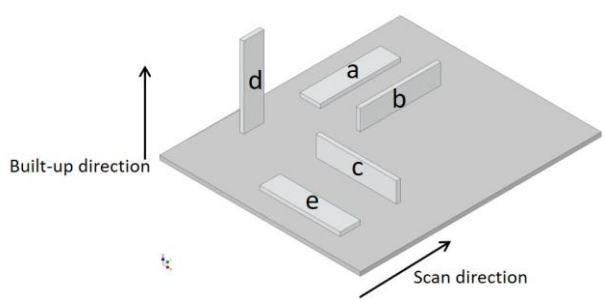

Fig. 1. Directions of manufactured tensile strength samples with relation to build-up to scanning orientations

It can be seen in Figure 1 above, that these layer orientations always contain one linear orientation corresponding with the scanning or welding direction. When analysing material anisotropies and material characteristics, usually angled orientations, such as e.g. 45° cut orientations are considered as well. For the DED process, these orientations are not relevant, as with the goal of minimal post-process shape milling, such angled layer orientations can not be generated and are therefore not content of the presented analysis.
The following Table 1 displays the used different materials with their material characteristics according to the

material data sheet. One major task within these described tests is the examination, whether the DED process has a significant impact on these as ideal considered material values, especially with respect to different layer orientations.

Table 1. Theoretic material parameters according to material data sheets

Powder	Material	Hardness	Tensile Strength
Metco 42C	1.4057 / X17CrNi16-2	271 HV0.3 (Spray coated)	850-1000 MPa
Metco 52C-NS	3.2581 / AlSi12	120 – 130 HV0.3 (spray coated)	150-200 MPa
Eutroloy 16.670	1.4370 / X10 CrNiMn18-8	160 HV30	600-650 MPa

Due to the layered structure resulting from the manufacturing process, flat specimens according to DIN 50125:2016-12 of tensile specimen shape E were selected. The cross-sectional area is chosen so that the maximum tensile force for the steel alloy based on the tensile strength from the data sheet is a maximum of 30 kN. The selected dimensions have a width of 3 mm, a thickness of 3 mm and a free length of 30 mm.
The tests were carried out in accordance with DIN EN ISO 6892-1 on a Galdabini QUASAR 100, which has wedge jaws for load application. Since the tensile specimens become very hard, aluminium glue had to be bonded to them at the load application points to prevent them from slipping. A tensile speed of 2 mm/min was specified. The universal testing machine records the applied force and the corresponding crosshead travel. Figure 2 shows this test setup (left) with the used tensile test specimen geometry (right).

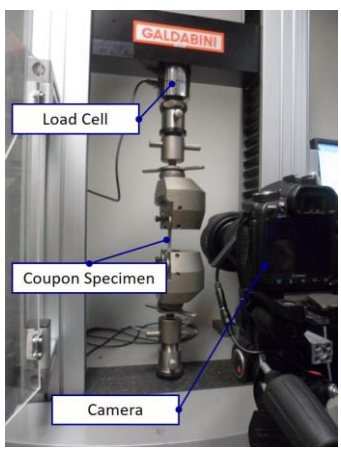

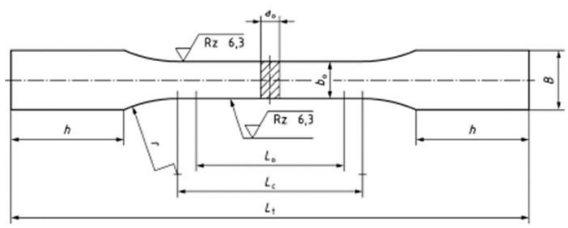

$a_0 = 3\ mm$ $B_{min} = 12\ mm$
$b_0 = 8\ mm$ $r_{min} = 12\ mm$
$L_0 = 30\ mm$ $h_{min} = 26\ mm$
$L_{c,min} = 38\ mm$
$L_{t,min} = 104\ mm$

Fig. 2. Test set-up (left) and used tensile test specimen geometry (right)

A speckle pattern was applied to the specimens and recorded at regular intervals during the test using a digital camera. Digital Image Correlation (DIC) can be used to assign strain to the individual time increments using the freely available GOM Correlate software. For some the flat specimens, strain gauges were additionally applied individually to check the results of the DIC. In average, each layer orientation and each material used have been tested with five individual flat test samples. The graphical results of the tensile tests with respect to their different layer orientation are depicted in the following figure 3 for the 1.4057 / X17CrNi16-2, in Figure 4 for the 1.4370 / X10 CrNiMn18-8 and in Figure 5 for the 3.2581 / AlSi12.

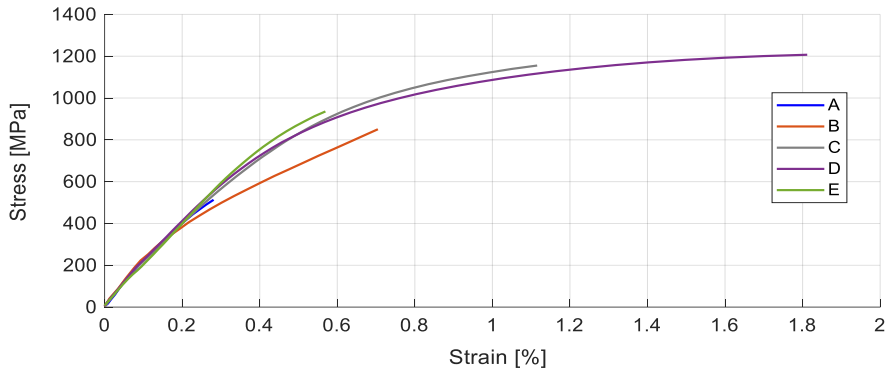

Fig. 3. Tensile test results for stress to strain relation for 1.4057 / X17CrNi16-2 steel base material

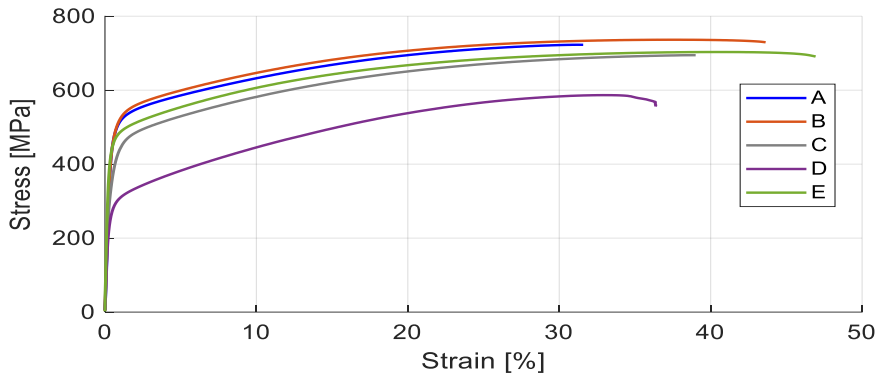

Fig. 4. Tensile test results for stress to strain relation for 1.4370 / X10 CrNiMn18-8 steel base material

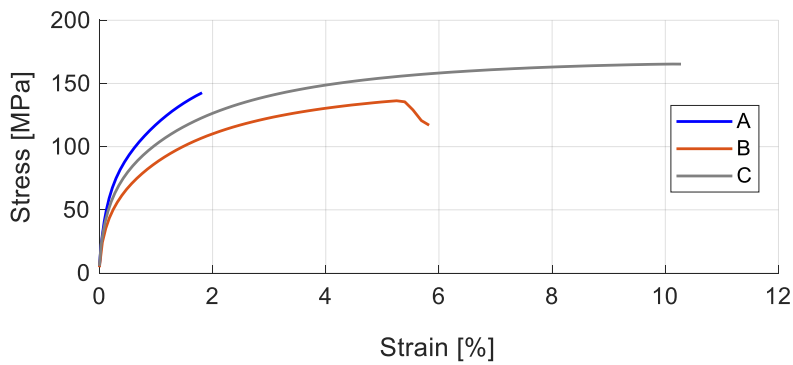

Fig. 5. Tensile test results for stress to strain relation for .2581 / AlSi12 aluminium base material

It can clearly be seen, that the individual test samples within one classification group and therefore layer orientation form a significant and homogenous result. It can also be seen, that there are severe differences in the ductility and breaking force when analysing the different materials. The pulling test results for the Young's modulus, the yield point, tensile strength, fracture elongation and Possion number are numerically displayed in the following Table 2.

Table 2. Data

Material	Orientation	Young's modulus [GPa]	Yield point [MPa]*	Tensile strength [MPa]	Fracture elongation [%]	v [%]
1.4057 / X17CrNi16-2†	A	195.8 ±24.8	395 ± 54	518 ±74	0.04 ±0.05	0.29 ±0.22
1.4057 / X17CrNi16-2	B	214.5 ±11.4	392 ±38	791 ±172	0.25 ±0.13	0.34 ±0.13
1.4057 / X17CrNi16-2	C	202.9 ±8.3	476 ±67	814 ±340	0.40 ±0.54	0.22 ±0.04
1.4057 / X17CrNi16-2	D	216.2 ±13.7	540 ±87	1119 ±243	1.00 ±0.69	0.27 ±0.03
1.4057 / X17CrNi16-2	E	213.4 ±19.8	700 ±71	1139 ±185	0.57 ±0.55	0.28 ±0.03
1.4370 / X10 CrNiMn18-8‡	A	148.9 ±23.2	460 ± 16	720 ± 9	40.68 ±8.6	0.27 ±0.13
1.4370 / X10 CrNiMn18-8	B	157.0 ± 7.7	460 ± 7	735 ± 3	44.49 ± 1.07	0.33 ± 0.06
1.4370 / X10 CrNiMn18-8	C	182.6 ± 41.0	362 ± 37	696 ± 6	45.22 ± 4.63	0.58 ± 0.18
1.4370 / X10 CrNiMn18-8	D	111.0 ± 2.8	273 ± 16	587 ± 4	37.58 ± 3.12	0.45 ± 0.04
1.4370 / X10 CrNiMn18-8	E	180.2 ± 24.7	442 ± 3	703 ± 3	47.96 ± 1.36	0.29 ± 0.09
3.2581 / AlSi12§	A	74.9 ± 10.5	77 ± 8	150 ± 21	2.51 ± 1.05	0.38 ± 0.15
3.2581 / AlSi12	B	40.8 ± 12.1	59 ± 6	82 ± 24	8.65 ± 4.00	0.50 ± 0.10
3.2581 / AlSi12	C	56.4 ± 5.9	68 ± 6	166 ± 6	15.51 ± 3.34	0.39 ± 0.04

For all specimens of the 1.4057 / X17CrNi16-2, an average Young's modulus of 195.8 GPa to 216.2 GPa is obtained. This value is thus in the range that is also achieved with the selected material in conventional processing (215 GPa). Furthermore, there is no anisotropic material behaviour for stiffness. Tensile strength, on the other hand, exhibited anisotropic material behaviour. In contrast to literature, compare Wolff et al. 2017 and Saboori et al. 2020, this is not characterized by the scan direction (orientation A and B). Instead, the anisotropy present is strongly influenced by the temperature history. In the flat orientation of A, for example, very fast cooling rates are present, so that a higher martensite formation occurs as expected according to the related data sheets. Orientation D, on the other hand, has comparatively long cooling times, which allow higher ductility and tensile strength. Specimen orientations B, C and E lie between orientations A and D in terms of ductility. Although orientation E is also flat like orientation A, comparatively high ductility and very high tensile strength are achieved with orientation E. This is due to the fact that the orientation E has a comparatively long cooling time. This origins from to the fact that the laser travels relatively short distances and thus more frequently over the specimen compared to specimen orientation A. As a result, annealing

* For the 1.4057/ X17CrNi16-2 samples, the 0.02% offset yield length was used due to the minimal plasticity

† Sample size n=6

‡ Sample size n= 4

§ Sample size n=3

effects occur. This results in tempering effects. All fracture surfaces were analysed under a microscope. In less than one fifth of the samples, pores can be seen in the fracture surface. The detected pores have diameters of 0.6 mm and 0.4 mm, respectively, and indicate gas entrapment. According to Caroll et al., 2015 and Wolff et al., 2017, these have no influence on the anisotropy. This fact as well as the low occurrence of pores support the thesis that the temperature history is significantly responsible for the anisotropy. However, comparable strength values can be achieved as with conventional processing.

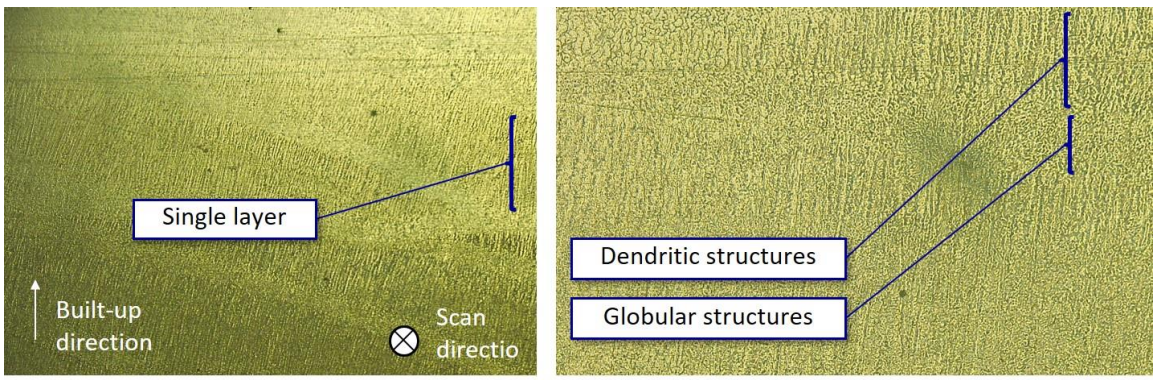

Fig. 6. Microscopic imaging of layer-cross section, with 100x magnification (left) and 300x magnification (right) for 1.4057 / X17CrNi16-2

In Figure 6 above, the analysis of the microstructure of a 1.4057 / X17CrNi16-2 sample in orientation A is shown. From bottom to top, the build-up direction of the cladded specimen can be seen. The viewing direction in the plane corresponds to the scan direction of the laser. A multilayer structure is visible by the alternating sequence of different solidification morphologies (elongated areas and short areas) from bottom to top. Likewise single tracks in one layer can be distinguished by those alternating morphologies from the left to right hand side. The second figure shows the magnification of the cross section and illustrates the different solidification morphologies in detail, which are already recognizable in Figure 6. These can be classified into globular (equiaxed) crystals and columnar crystals with a dendritic front. The difference can be explained with the solidification speed or the ratio of the speed of the solidification front *v* to the temperature gradient *G*. The relationship is described by the equation 1, compare Ilschner et al., 2016.

$$v * G = \frac{dT}{dt} \qquad (1)$$

The temperature gradient is greatest in the region of the base body (bottom), so that a dendritic structure is formed with a corresponding cooling rate and unstable solidification front. The further the melt moves away from the base body, the lower is the temperature gradient gets. Therefore, the morphology changes there to a globular crystal structure also shown by Ju et al., 2018. These microstructures, produced during laser cladding, are typical for cast microstructures.

With respect to the gathered data for the 1.4370 / X10 CrNiMn18-8 material, several facts need to be stated in particular. At first, a very high ductility can be observed, compare Figure 3 and Table 2. Additionally, a very low Young's modulus has been measured, with one reason being the relatively small elastic section as well as the low sampling rate of the DIC, which might not create enough measurement points for a valid Young's modulus quantification. In total, the measured values contain a very small scattering range on the one hand

within one orientation, but also within different orientations. In general, specimens which are tested with the force applied in direction of the scanning direction present themselves with the highest strength values. This also complies with the pertinent literature of Wolff et al. 2017 and Saboori et al. 2020. These strength values are comparable to the processing parameters compared to specimens being manufactured with conventional processing techniques.

For the 3.2581 / AlSi12 material, the fracture elongation and tensile strength values measured within the comparable too the data sheet values. Nevertheless, the Young's modulus measured for the B and C orientations are significantly too low as required for the manufacturing of complex, high strength and light-weight materials.

4. Conclusion and outlook

As a conclusion of this contribution, it can be said, that especially for the steel base materials similar material performance parameters can be achieved as with conventional manufacturing. In order to generate parts with the highest strength to weight ratio, parts should be manufactured with the main stress direction being oriented towards the main layer scanning orientation. As the measurement results display, even with aluminium being much more light weight than steel materials, the Young's modulus to weight ratio for Aluminium DED parts is significantly lower than for steel base materials. This is mainly due to the reason of missing heat treatment after the manufacturing, leading to aluminium material characteristics much closer to cast material as towards standard material.

Furthermore, a significant anisotropic behaviour of the DED manufactured parts can be observed. In order to predict the behaviour of more complex parts, the data described in this contribution can be used for a further Design-by-Feature approach, enabling a closer quantification of the anisotropy within the parts.

As an outlook for the manufacturing of individualized, large-sized DED-parts, further knowledge about the process and material behaviour, especially with respect to heat-induced stress deformation needs to be gathered. As all different and individual structures can be decomposed into individual design features, such as e.g. three- or four-way crossing points, linear structures, curved structures or circular structures, a Design-by-Feature based approach is to be suggested. By deriving all relevant design features by closely analysing the to be manufactured final parts, standardized procedures for these design features can iteratively be developed. This includes an optimisation of the process parameters and seam planning strategy in order to minimize heat-induced stress deformations as well as complete and parametrized machine programs, enabling a composition of complex DED-parts based on a modular Design-by-Feature processing catalogue.

Acknowledgements

The acknowledgements being relevant for this contribution are based on the research project *DEPOSE – Additive Fertigung von Kabinenmonumenten mittels Direct Energy Deposition (20Q1905)*, funded by the Federal Ministry for economic Affairs and energy (BMWi) within the 6th civil aviation research program (Luftfahrtforschungsprogramm, LuFo VI-1), controlled by the Projekt Management Agency for Aeronautics Research (Projektträger Luftfahrtforschung, PT-LF).

References

Bikas, H., Lianos, A. K., & Stavropoulos, P., 2019. A design framework for additive manufacturing. The International Journal of Advanced Manufacturing Technology, 1-15.

Carroll, B. E.; Palmer, T. A.; Beese, A. M., 2015. Anisotropic tensile behavior of Ti–6Al–4V components fabricated with directed energy deposition additive manufacturing, Acta Materialia, Vol. 87, pp. 309–320.

Castolin EuTroLoy 16.670 Data sheet, 2018. Metallpulver für Mischverbindugnen und Auftragungen.

Dass, A. & Moridi, A. (2019). State of the Art in Directed Energy Deposition: From Additive Manufacturing to Materials Design. Coatings, 9(7), p.418.

DIN 2020. Deutsches Institut für Normung e. V.DIN EN ISO 6892-1 - Metallische Werkstoffe – Zugversuch – Teil 1: Prüfverfahren bei Raumtemperatur, Metallische Werkstoffe – Zugversuch – Teil 1: Prüfverfahren bei Raumtemperatur, Beuth Verlag GmbH.

DIN Deutsches Institut für Normung e. V. LST: DIN 50125 - Prüfung metallischer Werkstoffe – Zugproben, Prüfung metallischer Werkstoffe – Zugproben, Beuth Verlag GmbH, Berlin, 2016.

Farayibi, P. K., Abioye, T. E., Kennedy, A., & Clare, A. T., 2019. Development of metal matrix composites by direct energy deposition of 'satellited'powders. Journal of Manufacturing Processes, 45, pp. 429-437.

Gibson, I.; Rosen, D. W.; Stucker, B.: Additive manufacturing technologies – Rapid prototyping to direct digital manufacturing, Springer, New York, 2010.

Ilschner, B., Singer, R.F., 2016. Werkstoffwissenschaften und Fertigungstechnik, 6. Aufl., Springer, Berlin.

Imran, M. K., Masood, S. H., Brandt, M., Bhattacharya, S. & Mazumder, J., 2011. Direct metal deposition (DMD) of H13 tool steel on copper alloy substrate: Evaluation of mechanical properties. Materials Science and Engineering: A, 528(9), pp. 3342–3349.

Ju, Jiang; Zhou, Yang; Kang, Maodong; Wang, Jun. 2018. "Optimization of Process Parameters, Microstructure, and Properties of Laser Cladding Fe-Based Alloy on 42CrMo Steel Roller" Materials 11, no. 10: 2061.

Kovacs, T., 2018. Laser welding process specification based on welding theories. Procedia Manufacturing, 22, pp. 147-153.

Liu, R., Wang, Z., Sparks, T., Liou, F., & Newkirk, J., 2017. Aerospace applications of laser additive manufacturing. In Laser additive manufacturing, pp. 351-371.

Oerlikon Metco 42C Data sheet, 2017. Material Product Data Sheet, Martensitic Stainless Steel Powders for Thermal Spray.

Oerlikon Metco 52C-NS Data sheet, 2016. Material Product Data Sheet, Aluminium 12% Silicon Thermal Spray Powders.

Saboori, A.; Aversa, A.; Marchese, G.; Biamino, S.; Lombardi, M.; Fino, P.: Microstructure and Mechanical Properties of AISI 316L Produced by Directed Energy Deposition-Based Additive Manufacturing: A Review, Applied Sciences, Vol. 10 (9), 2020, pp. 3310, https://doi.org/10.3390/app10093310.

Wang, Z.; Palmer, T. A.; Beese, A. M., 2016. Effect of processing parameters on microstructure and tensile properties of austenitic stainless steel 304L made by directed energy deposition additive manufacturing, Acta Materialia, Vol. 110, pp. 226–235.

Weaver, J. M., Barton, T. J., Linn, J., Jenkins, D., Miles, M. P., & Smith, R., 2019. Quantifying accuracy of a concept laser metal additive machine through the NIST test artifact. Rapid Prototyping Journal, 25(2), pp. 221-231.

Wolff, S. J.; Lin, S.; Faierson, E. J.; Liu, W. K.; Wagner, G. J.; Cao, J., 2017. A framework to link localized cooling and properties of directed energy deposition (DED)-processed Ti-6Al-4V, Acta Materialia, Vol. 132, pp. 106–117.

Wolff, S.; Lee, T.; Faierson, E.; Ehmann, K.; Cao, J.: Anisotropic properties of directed energy deposition (DED)-processed Ti–6Al–4V, Journal of Manufacturing Processes, Vol. 24, 2016, pp. 397–405, https://doi.org/10.1016/j.jmapro.2016.06.020.

Zhang, Y., Wu, L., Guo, X., Kane, S., Deng, Y., Jung, Y. G., & Zhang, J., 2018. Additive manufacturing of metallic materials: A review. Journal of Materials Engineering and Performance, 27(1), pp. 1-13.